ELSEVIER

Journal of Fluids and Structures 23 (2007) 351–363

JOURNAL OF FLUIDS AND STRUCTURES

www.elsevier.com/locate/jfs

A high dimensional harmonic balance approach for an aeroelastic airfoil with cubic restoring forces

L. Liu[a,*], E.H. Dowell[b], J.P. Thomas[b]

[a]Department of Mathematics, University of Texas Pan American, Edinburg, TX 78541, USA
[b]Department of Mechanical Engineering and Materials Science, Duke University, Durham, NC 27708, USA

Received 16 August 2005; accepted 28 September 2006
Available online 29 November 2006

Abstract

This is a study of a two-dimensional airfoil including a cubic spring stiffness placed in an incompressible flow. A new formulation of the harmonic balance method is employed for the aeroelastic airfoil to investigate the amplitude and frequency of the limit cycle oscillations. The results are compared with the results from the classical harmonic balance approach and from the conventional time marching integration method.

Keywords: High dimensional harmonic balance method; Airfoil; Cubic nonlinearity; Secondary bifurcation; Limit cycle oscillations

1. Introduction

Limit cycle oscillations (LCOs) and bifurcations arising from a concentrated structural nonlinearity in the restoring forces were first studied in Woolston et al. (1955) and Shen (1959). A comprehensive review of the bifurcations and chaos of the three basic nonlinearities, namely, cubic, freeplay and hysteresis has been reported recently in Lee et al. (1999b). The classical harmonic balance approach (Lee et al., 1997, 1999a) (including one dominant harmonic in the analysis) sometimes called the describing function (DF) approach or the equivalent linearization technique (Zhao and Yang, 1990) is often used to solve the equations of motion, but it cannot predict higher harmonic response (Price et al., 1995; Lee et al., 2003).

It is of fundamental scientific interest to understand the nonlinear system response beyond the onset of flutter. Moreover, in practice, some aircraft are operated beyond the flutter onset (e.g., the F-16). A major finding of the study in Liu and Dowell (2004) is that a surprisingly large number of harmonics is needed to describe the LCOs after the primary bifurcation for an airfoil with a cubic spring in the pitch degree of freedom. The high harmonics of the airfoil motions were investigated by a higher order harmonic balance approach (Liu and Dowell, 2004). While this approach generally yields accurate results for the amplitude and frequency of the LCOs, the algebra becomes very complex, and it is not an easy task to derive the analytical expressions for the Fourier components when many high harmonics are included in the analysis. Furthermore, this classical approach (called HB in this study) to the harmonic balance formulation is typically difficult to implement for complex systems of equations such as those arising from Euler and Navier–Stokes flows.

*Corresponding author. Tel.: +1 956 381 2578; fax: +1 956 384 5091.
E-mail address: LipingLiu@utpa.edu (L. Liu).

0889-9746/$ - see front matter
doi:10.1016/j.jfluidstructs.2006.09.005

Nomenclature

a_h	nondimensional distance from airfoil mid-chord to elastic axis
b	airfoil semi-chord
h	plunge displacement
m	airfoil mass
$\mathbf{I}$	identity matrix
r_α	radius of gyration about the elastic axis
t	time
x_α	nondimensional distance from the elastic axis to the center of mass
$C_L(\tau)$	aerodynamic lift coefficient
$C_M(\tau)$	aerodynamic pitching moment coefficient
n_h	number of harmonics used in harmonic balance method
$G(\xi)$	plunge stiffness term
$M(\alpha)$	nonlinear pitch stiffness term
Q	vector variable
U	free stream velocity
U^*	nondimensional velocity $U^* = U/b\omega_\alpha$
U_L^*	linear flutter speed
α	pitch angle of airfoil
β	constant in nonlinear pitch stiffness
ε_i	constant in Wagner's function, $i = 1, 2$
μ	airfoil/air mass ratio $\mu = m/\pi\rho b^2$
ξ	nondimensional plunge displacement $\xi = h/b$
ζ_α	viscous damping ratio in pitch
ζ_ξ	viscous damping ratio in plunge
τ	nondimensional time $\tau = Ut/b$
$\phi(\tau)$	Wagner's function
ψ_i	constant in Wagner's function, $i = 1, 2$
ω	frequency of the motion
$\bar{\omega}$	frequency ratio $\bar{\omega} = \omega_\xi/\omega_\alpha$

Subscripts

α	value for pitch angle
ξ	value for plunge deflection

Superscripts

$()'$	first derivative with respect to time τ
$()''$	second derivative with respect to time τ
$\hat{()}$	variables in frequency domain
$\tilde{()}$	variables in time domain

Recently, a new formulation (Thomas et al., 2002a,b; Hall et al., 2002) in terms of time-domain variables provides an alternative approach to the HB method. It is referred to as the high dimensional harmonic balance (HDHB) approach in this study. Instead of working in terms of the Fourier coefficient variables, the dependent variables in the HDHB system are the motion values at $2n_h + 1$ equally spaced sub-time levels over one cycle. The Fourier and time-domain variables are in fact related to one another via a constant Fourier transformation matrix. Working in terms of sub-time level variables circumvents the necessity of having to derive the analytical expressions of the Fourier coefficients required in the classical HB approach. In fact, the HDHB approach is easy to formulate within the framework of an existing time marching solver.

This is a follow-up study to that of Liu and Dowell (2004), focusing on a two-dimensional airfoil including a cubic spring force placed in an incompressible flow. The theoretical model is formulated as a set of first order ordinary differential equations. The HDHB approach is used to investigate the amplitude and frequency of the LCOs for the aeroelastic airfoil. The results are then compared with the results from the classical HB approach.

2. Model equations

A schematic of the typical airfoil section of the wing is shown in Fig. 1(a) and a cubic structural nonlinearity of the airfoil is shown in Fig. 1(b). There are two degrees of freedom: pitch angle α and plunge deflection ξ. For nonlinear restoring forces with incompressible subsonic aerodynamics, the coupled equations for the airfoil in nondimensional form are

$$\xi'' + x_a\alpha'' + 2\zeta_\xi \frac{\bar{\omega}}{U^*}\xi' + \left(\frac{\bar{\omega}}{U^*}\right)^2 G(\xi) = -\frac{1}{\pi\mu}C_L(\tau), \quad \frac{x_a}{r_\alpha^2}\xi'' + \alpha'' + 2\zeta_\alpha\frac{1}{U^*}\alpha' + \left(\frac{1}{U^*}\right)^2 M(\alpha) = \frac{2}{\pi\mu r_\alpha^2}C_M(\tau). \quad (1)$$

An approximation to the Wagner function (Lee et al., 1999b) is used to model the aerodynamic generalized forces $C_L(\tau)$ and $C_M(\tau)$. Four new variables (Lee et al., 1997) are introduced to eliminate the integral terms in the equations for the aeroelastic system:

$$w_1 = \int_0^\tau e^{-\varepsilon_1(\tau-\sigma)}\alpha(\sigma)\,d\sigma, \quad w_2 = \int_0^\tau e^{-\varepsilon_2(\tau-\sigma)}\alpha(\sigma)\,d\sigma, w_3 = \int_0^\tau e^{-\varepsilon_1(\tau-\sigma)}\xi(\sigma)\,d\sigma, \quad w_4 = \int_0^\tau e^{-\varepsilon_2(\tau-\sigma)}\xi(\sigma)\,d\sigma, \quad (2)$$

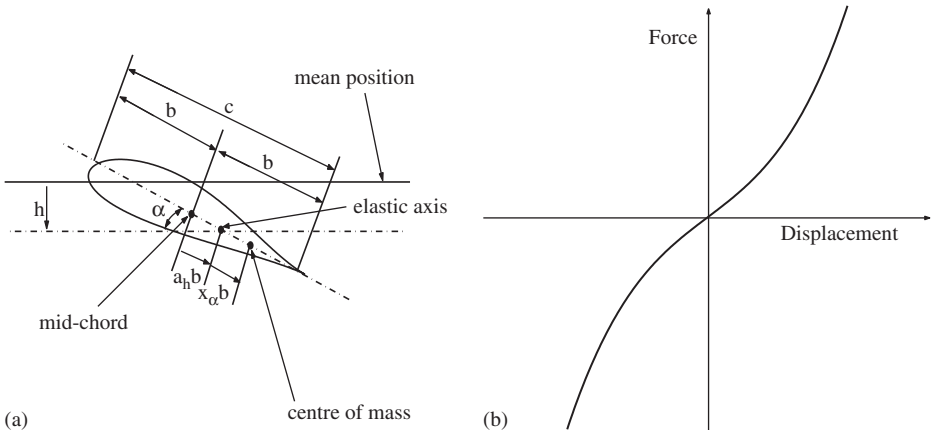

Fig. 1. (a) Two-degree-of-freedom airfoil motion; (b) cubic hardening spring.

where the Wagner function $\phi(\tau)$ is given by Jones' approximation (Jones, 1940):

$$\phi(\tau) = 1 - \psi_1 e^{-\varepsilon_1 \tau} - \psi_2 e^{-\varepsilon_2 \tau},$$

with the constants $\psi_1 = 0.165$, $\psi_2 = 0.335$, $\varepsilon_1 = 0.0455$, and $\varepsilon_2 = 0.3$. This study focuses on the hardening spring in the pitch degree of freedom. Therefore, the pitch and plunge stiffness are $M(x_1) = x_1 + \beta x_1^3$ and $G(x_3) = x_3$.

System (1) can then be rewritten in a general form containing only differential operators as

$$\begin{cases} c_0\xi'' + c_1\alpha'' + c_2\xi' + c_3\alpha' + (c_4 + c_{10})\xi + c_5\alpha + c_6 w_1 + c_7 w_2 + c_8 w_3 + c_9 w_4 = 0, \\ d_0\xi'' + d_1\alpha'' + d_2\xi' + d_3\alpha' + d_4\xi + d_5\alpha + d_6 w_1 + d_7 w_2 + d_8 w_3 + d_9 w_4 + d_{10}\alpha^3 = 0, \\ w_1' = \alpha - \varepsilon_1 w_1, \\ w_2' = \alpha - \varepsilon_2 w_2, \\ w_3' = \xi - \varepsilon_1 w_3, \\ w_4' = \xi - \varepsilon_2 w_4. \end{cases} \tag{3}$$

The coefficients $c_0, c_1, \ldots, c_{10}, d_0, d_1, \ldots, d_{10}$ are functions of system parameters, and the expressions are given in the Appendix.

3. Harmonic balance analysis

In the HB approach, the motions are assumed as their Fourier expansions with a finite number of harmonic terms:

$$\alpha(\tau) = \hat{\alpha}_0 + \sum_{n=1}^{n_h} [\hat{\alpha}_{2n-1} \cos(n\omega\tau) + \hat{\alpha}_{2n} \sin(n\omega\tau)], \quad \xi(\tau) = \hat{\xi}_0 + \sum_{n=1}^{n_h} [\hat{\xi}_{2n-1} \cos(n\omega\tau) + \hat{\xi}_{2n} \sin(n\omega\tau)],$$
$$w_i(\tau) = \hat{w}_0^i + \sum_{n=1}^{n_h} [\hat{w}_{2n-1}^i \cos(n\omega\tau) + \hat{w}_{2n}^i \sin(n\omega\tau)], \quad (i = 1, 2, 3, 4). \tag{4}$$

In vector form, the Fourier coefficients variables are

$$\hat{\mathbf{Q}}_\alpha = \begin{pmatrix} \hat{\alpha}_0 \\ \hat{\alpha}_1 \\ \vdots \\ \hat{\alpha}_{2n_h} \end{pmatrix}, \quad \hat{\mathbf{Q}}_\xi = \begin{pmatrix} \hat{\xi}_0 \\ \hat{\xi}_1 \\ \vdots \\ \hat{\xi}_{2n_h} \end{pmatrix}, \quad \hat{\mathbf{Q}}_{w_i} = \begin{pmatrix} \hat{w}_0^i \\ \hat{w}_1^i \\ \vdots \\ \hat{w}_{2n_h}^i \end{pmatrix}, \quad i = 1, 2, 3, 4.$$

Substituting (4) into system (1) and balancing the Fourier coefficients of the first n_h harmonics yields

$$\begin{cases} (c_0\omega^2\mathbf{A}^2 + c_2\omega\mathbf{A} + c_4\mathbf{I} + c_{10}\mathbf{I})\hat{\mathbf{Q}}_\xi + (c_1\omega^2\mathbf{A}^2 + c_3\omega\mathbf{A} + c_5\mathbf{I})\hat{\mathbf{Q}}_\alpha + \sum_{i=1}^4 c_{i+5}\hat{\mathbf{Q}}_{w_i} = \mathbf{0}, \\ (d_0\omega^2\mathbf{A}^2 + d_2\omega\mathbf{A} + d_4\mathbf{I})\hat{\mathbf{Q}}_\xi + (d_1\omega^2\mathbf{A}^2 + d_3\omega\mathbf{A} + d_5\mathbf{I})\hat{\mathbf{Q}}_\alpha + \sum_{i=1}^4 d_{i+5}\hat{\mathbf{Q}}_{w_i} + d_{10}\hat{\mathbf{M}}_\alpha = \mathbf{0}, \\ (\omega\mathbf{A} + \varepsilon_1\mathbf{I})\hat{\mathbf{Q}}_{w_1} - \hat{\mathbf{Q}}_\alpha = \mathbf{0}, \\ (\omega\mathbf{A} + \varepsilon_2\mathbf{I})\hat{\mathbf{Q}}_{w_2} - \hat{\mathbf{Q}}_\alpha = \mathbf{0}, \\ (\omega\mathbf{A} + \varepsilon_1\mathbf{I})\hat{\mathbf{Q}}_{w_3} - \hat{\mathbf{Q}}_\xi = \mathbf{0}, \\ (\omega\mathbf{A} + \varepsilon_2\mathbf{I})\hat{\mathbf{Q}}_{w_4} - \hat{\mathbf{Q}}_\xi = \mathbf{0}, \end{cases} \tag{5}$$

where $\mathbf{I}$ is an identity matrix with dimension $(2n_h+1)\times(2n_h+1)$, and $\hat{\mathbf{M}}_\alpha$ is for the Fourier components of α^3; $\mathbf{A}$ is a constant matrix related to n_h, and the expression is given in the Appendix. The last four equations in (5) for $\hat{\mathbf{Q}}_{w_i}$ $(i=1,2,3,4)$ can be easily solved. Substituting the results into the first two equations in (5) reduces the system to

$$\begin{cases} \mathbf{A}_1\hat{\mathbf{Q}}_\alpha + \mathbf{B}_1\hat{\mathbf{Q}}_\xi = \mathbf{0}, \\ \mathbf{A}_2\hat{\mathbf{Q}}_\alpha + \mathbf{B}_2\hat{\mathbf{Q}}_\xi + d_{10}\hat{\mathbf{M}}_\alpha = \mathbf{0}, \end{cases} \tag{6}$$

where $\mathbf{A}_i$ and $\mathbf{B}_i$ $(i=1,2)$ are $(2n_h+1)\times(2n_h+1)$ matrices with entries as functions of system parameters and the fundamental frequency ω. The expressions for $\mathbf{A}_i$ and $\mathbf{B}_i$ $(i=1,2)$ are in the Appendix. The first equation of system (6) can be solved as $\hat{\mathbf{Q}}_\xi = -\mathbf{B}_1^{-1}\mathbf{A}_1\hat{\mathbf{Q}}_\alpha$. The above HB system is then further reduced to a $2n_h+1$ dimensional system:

$$(\mathbf{A}_2 - \mathbf{B}_2\mathbf{B}_1^{-1}\mathbf{A}_1)\hat{\mathbf{Q}}_\alpha + d_{10}\hat{\mathbf{M}}_\alpha = \mathbf{0}. \tag{7}$$

The computation of the inverse for $\mathbf{B}_1$ is straightforward as the matrix is block diagonal. More details can be found in the Appendix.

For the hardening spring, the static motion is always zero. For LCOs, the phase of the first harmonic in pitch may be fixed at zero. Therefore, it can be assumed that $\hat{\alpha}_0 = 0$ and $\hat{\alpha}_1 = 0$. With this assumption, there are $2n_h$ equations in (7) and $2n_h$ unknowns including the fundamental frequency ω. The above system is solved in Liu and Dowell (2004) for n_h up to 17.

When n_h increases, it is difficult to obtain analytical expressions for the Fourier components of α^3 which are required in $\hat{\mathbf{M}}_\alpha$ in the HB system. This difficulty is overcome in the HDHB approach as the system is converted to the time domain with sub-time level variables:

$$\begin{cases} (c_0\omega^2\mathbf{G}^2 + c_2\omega\mathbf{G} + c_4\mathbf{I} + c_{10}\mathbf{I})\tilde{\mathbf{Q}}_\xi + (c_1\omega^2\mathbf{G}^2 + c_3\omega\mathbf{G} + c_5\mathbf{I})\tilde{\mathbf{Q}}_\alpha + \sum_{i=1}^4 c_{i+5}\tilde{\mathbf{Q}}_{w_i} = \mathbf{0}, \\ (d_0\omega^2\mathbf{G}^2 + d_2\omega\mathbf{G} + d_4\mathbf{I})\tilde{\mathbf{Q}}_\xi + (d_1\omega^2\mathbf{G}^2 + d_3\omega\mathbf{G} + d_5\mathbf{I})\tilde{\mathbf{Q}}_\alpha + \sum_{i=1}^4 d_{i+5}\tilde{\mathbf{Q}}_{w_i} + d_{10}\tilde{\mathbf{M}}_\alpha = \mathbf{0}, \\ (\omega\mathbf{G} + \varepsilon_1\mathbf{I})\tilde{\mathbf{Q}}_{w_1} - \tilde{\mathbf{Q}}_\alpha = \mathbf{0}, \\ (\omega\mathbf{G} + \varepsilon_2\mathbf{I})\tilde{\mathbf{Q}}_{w_2} - \tilde{\mathbf{Q}}_\alpha = \mathbf{0}, \\ (\omega\mathbf{G} + \varepsilon_1\mathbf{I})\tilde{\mathbf{Q}}_{w_3} - \tilde{\mathbf{Q}}_\xi = \mathbf{0}, \\ (\omega\mathbf{G} + \varepsilon_2\mathbf{I})\tilde{\mathbf{Q}}_{w_4} - \tilde{\mathbf{Q}}_\xi = \mathbf{0}, \end{cases} \tag{8}$$

where $\mathbf{G} = \mathbf{E}^{-1}\mathbf{A}\mathbf{E}$ is a constant matrix related to the Fourier transform matrix $\mathbf{E}$. The expressions for $\mathbf{E}$ and $\mathbf{E}^{-1}$ are given in the Appendix. The time domain solutions are given as follows:

$$\tilde{\mathbf{Q}}_\alpha = \begin{pmatrix} \alpha(t_0) \\ \alpha(t_1) \\ \vdots \\ \alpha(t_{2n_h}) \end{pmatrix}, \quad \tilde{\mathbf{Q}}_\xi = \begin{pmatrix} \xi(t_0) \\ \xi(t_1) \\ \vdots \\ \xi(t_{2n_h}) \end{pmatrix}, \quad \tilde{\mathbf{M}}_\alpha = \begin{pmatrix} \alpha^3(t_0) \\ \alpha^3(t_1) \\ \vdots \\ \alpha^3(t_{2n_h}) \end{pmatrix},$$

and $t_i = i2\pi/(2n_h+1)$, $(i=0,1,2,\ldots,2n_h)$. System (8) is easy to implement in a computer program, and requires only the rearrangement of the arrays in a conventional time-marching integration program. From the study in Liu et al. (2006) the equivalent system of the HDHB system in the frequency domain may be obtained by simply replacing the nonlinear term $\hat{\mathbf{M}}_\alpha$ in (7) by $\mathbf{E}(\mathbf{E}^{-1}\hat{\mathbf{Q}}_\alpha)^3$:

$$(\mathbf{A}_2 - \mathbf{B}_2\mathbf{B}_1^{-1}\mathbf{A}_1)\hat{\mathbf{Q}}_\alpha + d_{10}\mathbf{E}(\mathbf{E}^{-1}\hat{\mathbf{Q}}_\alpha)^3 = \mathbf{0}. \tag{9}$$

Although system (9) is in the frequency domain, the difficult part of the HB approach, i.e., the algebraic computation of the individual Fourier component of α^3, is avoided. Therefore, the computation time in the HDHB method is less than that in the HB method, and the difference becomes more significant when many high harmonics are included in the investigation. Similar to the procedure in obtaining the HB solutions, $\hat{\alpha}_1$ is assumed zero. System (9) is then solved for $\hat{\alpha}_i$ ($i = 0, 2, 3, \ldots, 2n_h$) and the response frequency ω.

4. Results and discussions

In this study, the system parameters under consideration are $\mu = 100$, $r_\alpha = 0.5$, $a_h = -0.5$, $\zeta_\alpha = \zeta_\xi = 0$, $\bar{\omega} = 0.2$, $x_\alpha = 0.25$ and $\beta = 80$. The detailed results from the conventional time marching and HB methods for this case have been obtained in a previous study (Liu and Dowell, 2004). The main interest is the secondary bifurcation for a velocity ratio (flow velocity over linear flutter speed) near 2. The response frequency decreases continuously before the secondary bifurcation, then drops rapidly from 0.06 to 0.04 at the secondary bifurcation, and then the frequency remains at 0.04 for larger velocities. At the secondary bifurcation, besides the rapid increasing of the amplitude, the motion type for the pitch angle changes from one peak per cycle to three peaks per cycle. The plunge motion remains one peak per cycle while the amplitude is almost doubled for a velocity ratio near 2. It is found in previous study (Liu and Dowell, 2004) that nine harmonics have to be included in the HB analysis in order to detect the secondary bifurcation.

The numerical time marching results reported here are obtained by using the fourth order Runge–Kutta scheme, and the initial condition is $\alpha(0) = 1.0^\circ$ and $\alpha'(0) = \xi(0) = \xi'(0) = 0$. The results are shown in Figs. 2–10 as open circles to

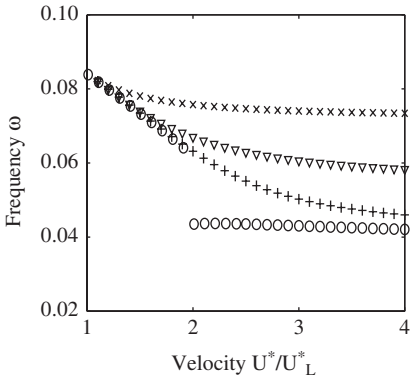

Fig. 2. The frequency ω from the HB method with various numbers of harmonics included in the analysis, in comparison with the time marching results: ×, HB1; ∇, HB3; +, HB5; ○, time marching.

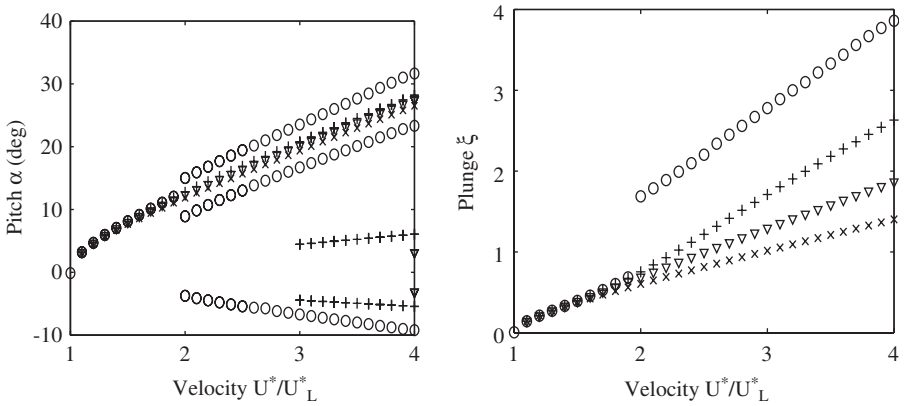

Fig. 3. Pitch and plunge peak values from the HB method with various numbers of harmonics, in comparison with the time marching results. The symbols are the same as those in Fig. 2.

compare with the HB and HDHB methods with various numbers of harmonics. In these figures, all the variables are non-dimensional except the pitch angle α which is converted to degree.

For the computation of the HB and HDHB solutions, the velocity ratio increases gradually from 1 to 4, while the solution from the lower velocity is used as the initial starting solution for the nonlinear solver. For the motions before the secondary bifurcation, the increment in flow velocity could be relatively large, e.g., 0.1. The size of the increment velocity becomes crucial for the motions near the secondary bifurcation. For example, for the HDHB solutions with 14 harmonics included in the system, the incremental step needs to be 0.0001 for the flow velocities near the secondary bifurcation.

4.1. HB results

The HB solutions for the amplitudes of the zeroth and even harmonics are zero. Therefore, the HB results with an odd number of harmonics are reported. The frequency solutions from the HB system with one harmonic (HB1), three harmonics (HB3) and five harmonics (HB5) are displayed in Fig. 2, in comparison with the time marching results denoted by open circles. The HB1 solutions denoted by crosses decrease very slowly and remain above 0.07 when the velocity increases. The discrepancy of the HB1 approximation from the time marching motions becomes evident for a velocity ratio near 1.2, and the deviation enlarges as the velocity increases. The HB3 solutions denoted by triangles improve upon the HB1 results as the deviation starts to appear for a velocity ratio near 1.4. Nonetheless, the HB3 curve is smooth and remains above 0.06. The HB5 solutions denoted by pluses match well with the time marching motions before the secondary bifurcation, i.e., $U^*/U_L^* = 2$. However, the HB solutions in Fig. 2 are smooth and do not detect the secondary bifurcation.

The pitch and plunge amplitudes from the HB1, HB3 and HB5 for the motions before the secondary bifurcation are close and match the time-marching results well, as shown in Fig. 3. For the pitch motion, the amplitudes from HB1, HB3 and HB5 solutions remain the same and keep increasing gradually for the velocity after the secondary bifurcation, except that two more peaks per cycle occur for the HB5 motions for velocities beyond $3U_L^*$. For the plunge motion, the difference between the HB1, HB3 and HB5 solutions becomes large for velocities beyond the secondary bifurcation. Nonetheless, no jump has been detected in the amplitudes of the pitch and plunge motions, which is consistent with the frequency response.

The results shown in Fig. 4 from the HB method with seven harmonics (HB7) included in the analysis begin to show the evidence of the secondary bifurcation. Two continuous curves are found in the frequency response. One decreases gradually from 0.090 to 0.038. The other curve covers the straight line 0.042, which is the frequency curve for the motions after the secondary bifurcation. However, the latter curve, which has not been discovered in previous study (Liu and Dowell, 2004), is very hard to obtain, as the appropriate initial starting points for the nonlinear solver are within a narrow range. Consistent with the frequency prediction curve, parts of the pitch amplitudes from the HB7 solutions match the time-marching results.

The HB solutions with nine harmonics (HB9) clearly detect the secondary bifurcation, and the results are shown in Fig. 5 for the frequency, pitch and plunge motions in comparison with the time marching results. For the frequency, first the HB9 solution decreases as the velocity increases, until it reaches the value 0.042, it then decreases and increases as the velocity decreases from $2.3U_L^*$ to $1.85U_L^*$. Finally at $U^*/U_L^* = 1.85$ it turns back to 0.042 and remains on the straight line for U^* up to $4U_L^*$. The HB9 prediction for the frequency is a single twisted curve, and it detects the secondary bifurcation, and matches the time marching results well for the motions before and after the secondary bifurcation. Correspondingly, the HB9 solutions for the pitch and plunge motions amplitudes also detect the secondary bifurcation and match the time marching results well.

4.2. HDHB results

The HDHB solutions for the coefficients of the zeroth and eventh harmonics are usually nonzero. Therefore, unlike the HB solutions, the solutions from the HDHB method with one harmonic (HDHB1) are different from the HDHB solutions when two harmonics are included (HDHB2), which are different from the HDHB solutions when three harmonics are included (HDHB3). Overall, the more harmonics included in the HDHB system, the more accurate the HDHB solutions are. Compared to the HB solutions, the HDHB solutions when $2n$ harmonics are included in the analysis (HDHB2n) are close to the HB solutions when n harmonics are included (HBn), while the HDHB solutions when less than $2n$ harmonics are included are usually less accurate than the HB solutions when n harmonics are included.

The frequency solutions from the HDHB method with two harmonics (HDHB2), six harmonics (HDHB6) and 10 harmonics (HDHB10) are displayed in Fig. 6. The results from the HDHB method with one harmonic (HDHB1) are

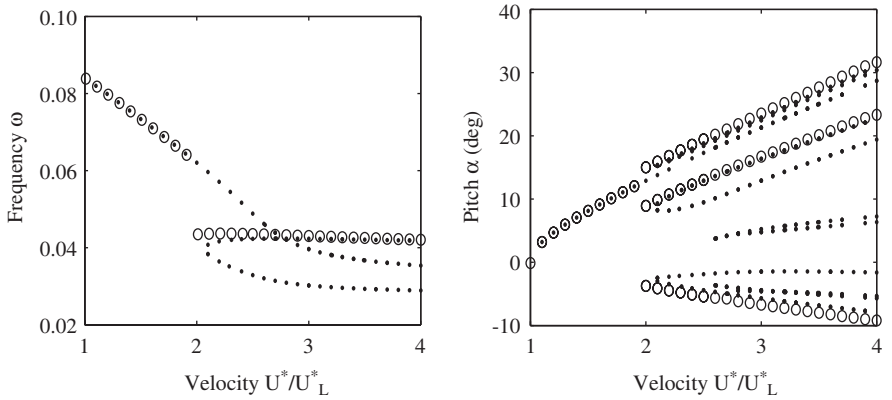

Fig. 4. The frequency ω and pitch peak values from the HB method with seven harmonics, in comparison with the time-marching results: ○, time marching; ·, HB7.

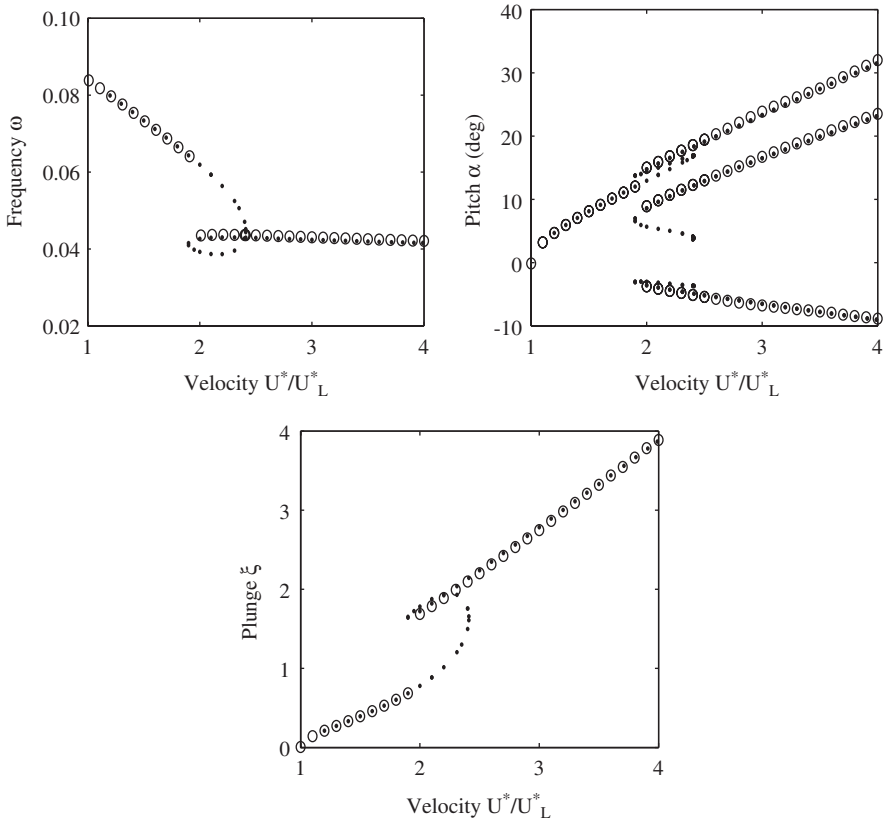

Fig. 5. The frequency, pitch and plunge peak values from the HB method with nine harmonics, in comparison with the time-marching results: ○, time marching; ·, HB9.

above the HDHB2 solutions denoted by crosses in Fig. 6. The HDHB results from the HDHB method with three, four and five harmonics are above the HDHB6 solutions denoted by triangles and below the HDHB2 solutions by cross in Fig. 6. Similarly, the results from the HDHB method with seven, eight and nine harmonics are between the HDHB6 and HDHB10 solutions. Comparing the HDHB solutions in Fig. 6 with the HB solutions in Fig. 2, one finds that the HDHB2 solutions are close to the HB1 solutions, the HDHB6 solutions are close to the HB3 solutions, and the

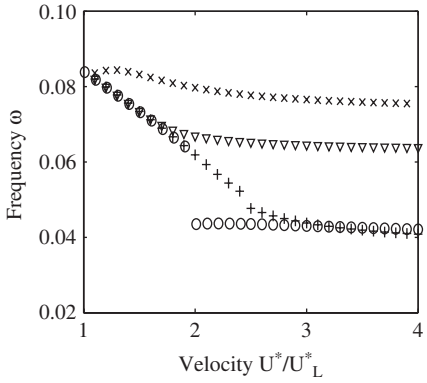

Fig. 6. The frequency ω from the HDHB method with various numbers of harmonics, in comparison with the time-marching results: $\times$, HDHB2; ∇, HDHB6; $+$, HDHB10; $\circ$, time marching.

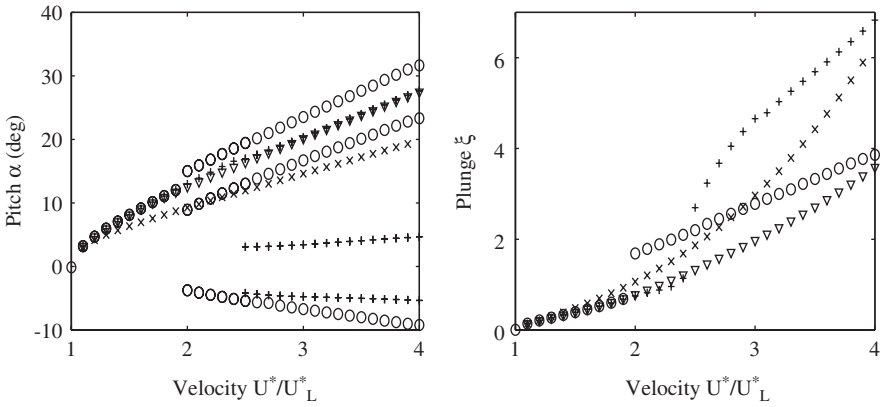

Fig. 7. Pitch and plunge peak values from the HDHB method with various numbers of harmonics, in comparison with the time-marching results. The symbols are the same as those in Fig. 6.

HDHB10 solutions are close to the HB5 results. The HDHB2 results are a bit worse than the HB1 prediction, in the sense that the HDHB2 solution increases right after the primary bifurcation, while the HB1 solution decreases and follows the time-marching results. For the velocities before the secondary bifurcation, the HDHB6 solutions are bit better than those from the HB3 method. This is also true when the HDHB10 solutions are compared with the HB5 results.

Similar to the HB1 and HB3 solutions for the pitch and plunge motions amplitudes, the amplitudes from the HDHB2 and HDHB6, as shown in Fig. 7, also increase continuously for the velocities beyond the secondary bifurcation. From the HDHB10 solutions for the pitch motion peak values, the change of the motion type from one peak per cycle to three peaks per cycle starts to occur as early as $U^*/U_L^* = 2.5$, while this change does not occur until $U^*/U_L^* = 3.0$ in the HB5 solutions. Note that in Fig. 6 the frequency solutions from the HDHB10 method for velocities beyond $3U_L^*$ are close to the time-marching results, but the solutions for the amplitudes in Fig. 7 are very different from the time-marching results. Therefore, the secondary bifurcation is not captured by the HDHB method with less than 10 harmonics.

The HDHB solutions when 11, 12 and 13 harmonics are included in the analysis are not as accurate as the HB7 solutions. In particular, the motions after the secondary bifurcation cannot be captured by the HDHB method with the number of harmonics less than 14. Since there are two disconnected branches in the HB7 prediction and part of one branch does capture the motions after the secondary bifurcation, it is interesting to observe the HDHB solutions when 14 harmonics are included (HDHB14). The frequency, pitch and plunge motion peak values are shown in Fig. 8. The

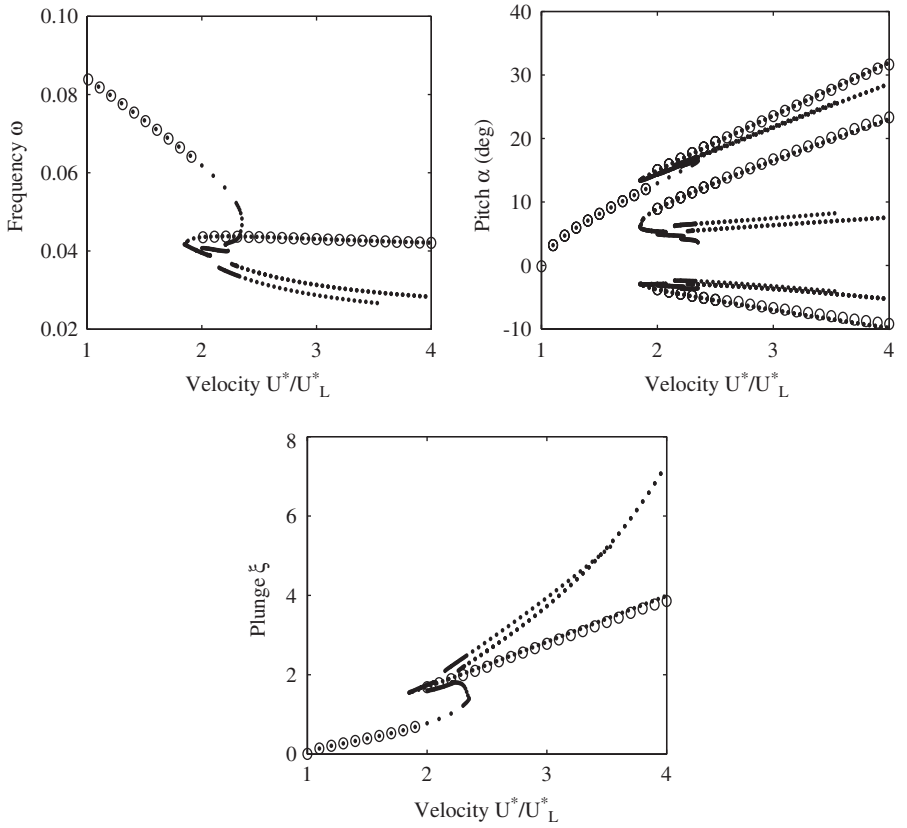

Fig. 8. The frequency, pitch and plunge peak values from the HDHB method with 14 harmonics, in comparison with the time-marching results: ○, time marching; ·, HDHB14.

structure of the HDHB14 solutions for velocities between $1.85U_L^*$ and $2.5U_L^*$ is complex, and the solutions are relatively difficult to obtain. To obtain a convergent solution from the nonlinear solver for solutions near the secondary bifurcation, the increment for the velocity ratio needs to be very small (0.001). From the frequency graph in Fig. 8, it seems that there is a branch that twists to a straight line at $\omega = 0.042$. However, a zoomed view shows us that there are two discontinuities in that curve. The discontinuities can hardly be seen in the pitch and plunge motion peak values. Nonetheless, the time-marching results for the motions after the secondary bifurcation are matched by some of the HDHB14 solutions, which is confirmed in the frequency and the motion peak values in Fig. 8.

Including one more harmonic in the HDHB method, i.e., HDHB15, improves upon the HDHB14 solutions (and thus the HB7 solutions) substantially. The results from the HDHB15 system are plotted in Fig. 9 for the frequency and the motion peak values. From the frequency graph, the HDHB15 prediction is a single twisted curve that covers all the time-marching results. However, the unstable branch in the hysteresis is not as smooth as that in the HB9 prediction. This is again confirmed in the HDHB15 solutions for the pitch and plunge motion peak values. The motions after the secondary bifurcation are successfully detected in the HDHB15 solutions. Furthermore, the HDHB15 solutions are easier to obtain, compared to the procedure in obtaining the HDHB14 solutions, in the sense that the appropriate initial starting points for the nonlinear solver are within a larger range.

The results from the HDHB method when 16 (HDHB16) or 17 harmonics (HDHB17) are included in the analysis are similar to the HDHB15 solutions. The HDHB solutions with 18 harmonics (HDHB18) are close to the HB9 solutions, where a clear single smooth twisted curve is found for the frequency prediction. The HDHB18 results are shown in Fig. 10 for the frequency and the motion peak values in comparison with the corresponding time marching results. For the frequency, the twisting loop is smaller than that in the HB9 prediction in Fig. 5. Comparing the HDHB18 results in Fig. 10 with the corresponding HB9 results in Fig. 5, we find that the HDHB18 results are more accurate than the HB9 solutions, in the sense that the HDHB18 solutions are closer to the time-marching results.

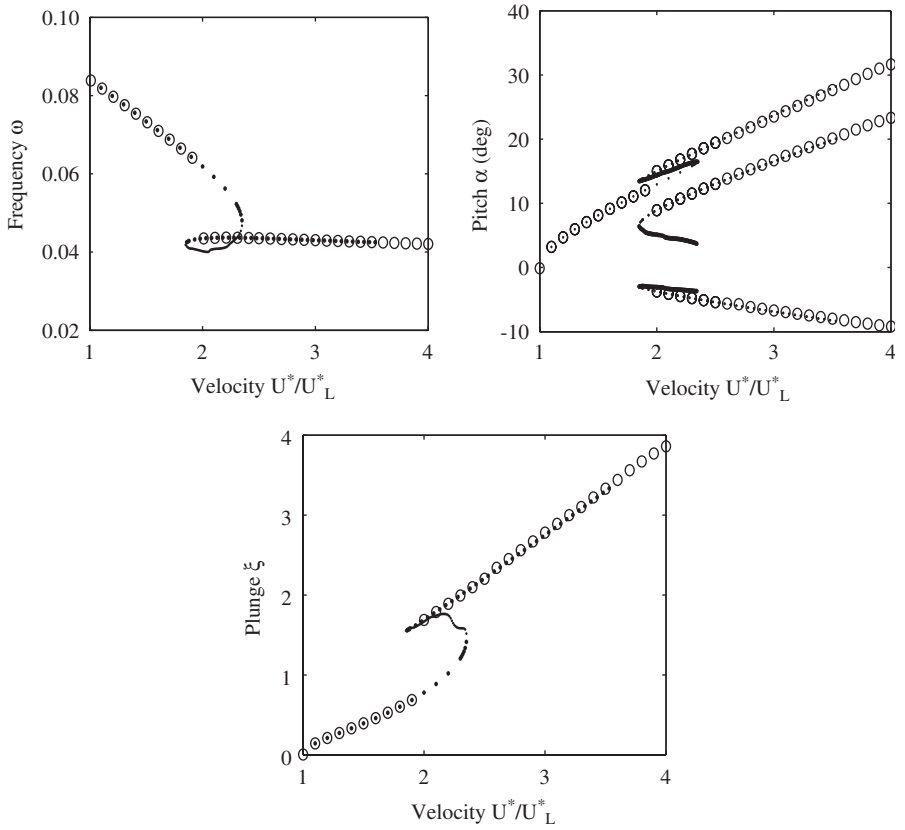

Fig. 9. The frequency, pitch and plunge peak values from the HDHB method with 15 harmonics, in comparison with the time-marching results: ○, time marching; ·, HDHB15.

5. Conclusions

For small amplitude motions near the primary bifurcation, the HDHB and HB solutions are close to the time-marching results. For the motions away from the primary bifurcation, the discrepancy between the time-marching results with the HB/HDHB solutions becomes significant. The more harmonics taken into consideration in the analysis, the more accurate are the results obtained from the HB/HDHB methods. The result from the classical HB method is more accurate than that from the HDHB method when the same number of harmonics are included in the analysis. In order to obtain the same order accuracy, the number of the harmonics included in the HDHB method needs to be twice the number included in the HB method. The fact that the results from the HDHB2*n* system are as accurate as those from the HBn system is due to the cubic nonlinearity. The number of harmonics needed in the HDHB method (for the solutions as accurate as those from the HB method) varies for different nonlinearities. For instance, for a quadratic nonlinearity, the number of the harmonics included in the HDHB method is less than twice the number included in the HB method for the same order accuracy. More details of this will be presented in a future study.

For the prediction of the secondary bifurcation which occurs for velocities almost twice the linear flutter speed, at least seven harmonics need to be included in the HB analysis, while 14 harmonics are needed in the HDHB analysis. To obtain a continuous transition (a clear loop in the prediction curve) from the primary bifurcation to the secondary bifurcation, nine harmonics are required in the HB analysis, while 15 harmonics are needed in the HDHB analysis.

On the other hand, the HB system is difficult to derive when the number of high harmonics is large, while the HDHB system is easy to derive and to implement into a computer program regardless of the number of harmonics included in the analysis. Since the variable in the HDHB analysis are the time domain solutions, this method is suitable and efficient for high dimensional systems with various nonlinearities, for which the HB method may be practically impossible to implement.

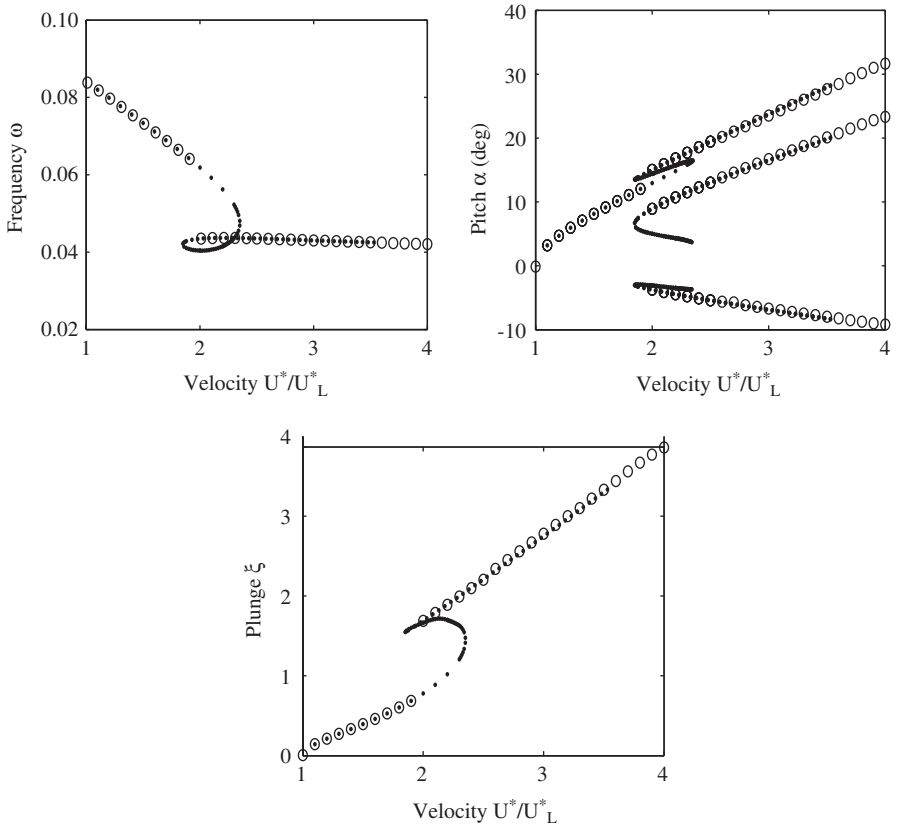

Fig. 10. The frequency, pitch and plunge peak values from the HDHB method with 18 harmonics, in comparison with the time-marching results: ○, time marching; ·, HDHB18.

Acknowledgments

This work was supported by the Faculty Research Council at the University of Texas Pan American, Edinburg, Texas, USA.

Appendix

The coefficients in Eq. (3) are:

$$c_0 = 1 + \frac{1}{\mu}, \quad c_1 = x_\alpha - \frac{a_h}{\mu}, \quad c_2 = 2\zeta_\xi \frac{\bar{\omega}}{U^*} + \frac{2}{\mu}(1 - \psi_1 - \psi_2),$$

$$c_3 = \frac{1}{\mu}(1 + (1 - 2a_h)(1 - \psi_1 - \psi_2)), \quad c_4 = \frac{2}{\mu}(\varepsilon_1\psi_1 + \varepsilon_2\psi_2),$$

$$c_5 = \frac{2}{\mu}(1 - \psi_1 - \psi_2 + \left(\frac{1}{2} - a_h\right)(\varepsilon_1\psi_1 + \varepsilon_2\psi_2)), \quad c_6 = \frac{2}{\mu}\varepsilon_1\psi_1\left(1 - \varepsilon_1\left(\frac{1}{2} - a_h\right)\right),$$

$$c_7 = \frac{2}{\mu}\varepsilon_2\psi_2\left(1 - \varepsilon_2\left(\frac{1}{2} - a_h\right)\right), \quad c_8 = -\frac{2}{\mu}\varepsilon_1^2\psi_1, \quad c_9 = -\frac{2}{\mu}\varepsilon_2^2\psi_2, \quad c_{10} = \left(\frac{\bar{\omega}}{U^*}\right)^2;$$

$$d_0 = \frac{x_\alpha}{r_\alpha^2} - \frac{a_h}{\mu r_\alpha^2}, \quad d_1 = 1 + \frac{1 + 8a_h^2}{8\mu r_\alpha^2}, \quad d_2 = -\frac{1}{\mu r_\alpha^2}(1 + 2a_h)(1 - \psi_1 - \psi_2),$$

$$d_3 = 2\zeta_\alpha \frac{1}{U^*} + \frac{1}{2\mu r_\alpha^2}(1 - 2a_h) - \frac{1}{2\mu r_\alpha^2}(1 + 2a_h)(1 - 2a_h)(1 - \psi_1 - \psi_2),$$

$$d_4 = -\frac{1}{\mu r_\alpha^2}(1+2a_h)(\varepsilon_1\psi_1+\varepsilon_2\psi_2),$$
$$d_5 = -\frac{1}{\mu r_\alpha^2}(1+2a_h)(1-\psi_1-\psi_2) - \frac{1}{2\mu r_\alpha^2}(1+2a_h)(1-2a_h)(\psi_1\varepsilon_1-\psi_2\varepsilon_2),$$
$$d_6 = -\frac{1}{\mu r_\alpha^2}(1+2a_h)\psi_1\varepsilon_1\left(1-\varepsilon_1\left(\frac{1}{2}-a_h\right)\right), \quad d_7 = -\frac{1}{\mu r_\alpha^2}(1+2a_h)\psi_2\varepsilon_2\left(1-\varepsilon_2\left(\frac{1}{2}-a_h\right)\right),$$
$$d_8 = \frac{1}{\mu r_\alpha^2}(1+2a_h)\psi_1\varepsilon_1^2, \quad d_9 = \frac{1}{\mu r_\alpha^2}(1+2a_h)\psi_2\varepsilon_2^2, \quad d_{10} = \left(\frac{1}{U^*}\right)^2.$$

$\mathbf{A}$ is given by

$$\mathbf{A} = \begin{pmatrix} \mathbf{0} & & & & \\ & \mathbf{J}_1 & & & \\ & & \mathbf{J}_2 & & \\ & & & \cdots & \\ & & & & \mathbf{J}_{n_h} \end{pmatrix} \tag{10}$$

and

$$\mathbf{J}_n = n\begin{pmatrix} 0 & 1 \\ -1 & 0 \end{pmatrix}, \quad n = 1,2,\ldots,n_h.$$

Solving the first equation of (5) for $\hat{\mathbf{Q}}_\xi$ and substituting the solution into the second equation of (5) yields the reduced HB system (6), where

$$\mathbf{A}_1 = c_1\omega^2\mathbf{A}^2 + c_3\omega\mathbf{A} + c_5\mathbf{I} + c_8(\omega\mathbf{A}+\varepsilon_1\mathbf{I})^{-1} + c_9(\omega\mathbf{A}+\varepsilon_2\mathbf{I})^{-1},$$
$$\mathbf{A}_2 = d_1\omega^2\mathbf{A}^2 + d_3\omega\mathbf{A} + d_5\mathbf{I} + d_8(\omega\mathbf{A}+\varepsilon_1\mathbf{I})^{-1} + d_9(\omega\mathbf{A}+\varepsilon_2\mathbf{I})^{-1},$$
$$\mathbf{B}_1 = c_0\omega^2\mathbf{A}^2 + c_2\omega\mathbf{A} + c_4\mathbf{I} + c_6(\omega\mathbf{A}+\varepsilon_1\mathbf{I})^{-1} + c_7(\omega\mathbf{A}+\varepsilon_2\mathbf{I})^{-1},$$
$$\mathbf{B}_2 = d_0\omega^2\mathbf{A}^2 + d_2\omega\mathbf{A} + d_4\mathbf{I} + d_6(\omega\mathbf{A}+\varepsilon_1\mathbf{I})^{-1} + d_7(\omega\mathbf{A}+\varepsilon_2\mathbf{I})^{-1}. \tag{11}$$

Denote $\mathbf{B}(\varepsilon) = \omega\mathbf{A} + \varepsilon\mathbf{I}$. From (10),

$$\mathbf{B}(\varepsilon) = \begin{pmatrix} \varepsilon & & & & \\ & \mathbf{L}_1(\varepsilon) & & & \\ & & \mathbf{L}_2(\varepsilon) & & \\ & & & \cdots & \\ & & & & \mathbf{L}_{n_h}(\varepsilon) \end{pmatrix}, \tag{12}$$

with

$$\mathbf{L}_n(\varepsilon) = \begin{pmatrix} \varepsilon & n\omega \\ -n\omega & \varepsilon \end{pmatrix}, \quad n = 1,2,\ldots,n_h.$$

Therefore, the inverse of $\mathbf{B}$ is $\mathbf{C}(\varepsilon) = \mathbf{B}^{-1}(\varepsilon)$:

$$\mathbf{C}(\varepsilon) = \begin{pmatrix} \frac{1}{\varepsilon} & & & & \\ & \mathbf{L}_1^{-1}(\varepsilon) & & & \\ & & \mathbf{L}_2^{-1}(\varepsilon) & & \\ & & & \cdots & \\ & & & & \mathbf{L}_{n_h}^{-1}(\varepsilon) \end{pmatrix}, \tag{13}$$

with

$$\mathbf{L}_n^{-1}(\varepsilon) = \frac{1}{\varepsilon^2+(n\omega)^2}\begin{pmatrix} \varepsilon & -n\omega \\ n\omega & \varepsilon \end{pmatrix}, \quad n = 1,2,\ldots,n_h.$$

Substituting (13) into (11) yields the expressions for $\mathbf{A}_i$ and $\mathbf{B}_i$ $(i = 1, 2)$:

$$\begin{aligned}
\mathbf{A}_1 &= c_1\omega^2\mathbf{A}^2 + c_3\omega\mathbf{A} + c_5\mathbf{I} + c_8\mathbf{C}(\varepsilon_1) + c_9\mathbf{C}(\varepsilon_2),\\
\mathbf{A}_2 &= d_1\omega^2\mathbf{A}^2 + d_3\omega\mathbf{A} + d_5\mathbf{I} + d_8\mathbf{C}(\varepsilon_1) + d_9\mathbf{C}(\varepsilon_2),\\
\mathbf{B}_1 &= c_0\omega^2\mathbf{A}^2 + c_2\omega\mathbf{A} + c_4\mathbf{I} + c_6\mathbf{C}(\varepsilon_1) + c_7\mathbf{C}(\varepsilon_2),\\
\mathbf{B}_2 &= d_0\omega^2\mathbf{A}^2 + d_2\omega\mathbf{A} + d_4\mathbf{I} + d_6\mathbf{C}(\varepsilon_1) + d_7\mathbf{C}(\varepsilon_2).
\end{aligned} \tag{14}$$

In system (8) and (9), $\mathbf{G} = \mathbf{E}^{-1}\mathbf{A}\mathbf{E}$, the Fourier transform matrix is

$$\mathbf{E} = \frac{2}{2n_h+1}\begin{pmatrix}
\frac{1}{2} & \frac{1}{2} & \dots & \frac{1}{2}\\
\cos t_0 & \cos t_1 & \dots & \cos t_{2n_h}\\
\sin t_0 & \sin t_1 & \dots & \sin t_{2n_h}\\
\cos 2t_0 & \cos 2t_1 & \dots & \cos 2t_{2n_h}\\
\sin 2t_0 & \sin 2t_1 & \dots & \sin 2t_{2n_h}\\
\vdots & \vdots & & \vdots\\
\cos n_h t_0 & \cos n_h t_1 & \dots & \cos n_h t_{2n_h}\\
\sin n_h t_0 & \sin n_h t_1 & \dots & \sin n_h t_{2n_h}
\end{pmatrix},$$

and $\mathbf{E}^{-1}$ is given by

$$\begin{pmatrix}
1 & \cos t_0 & \sin t_0 & \dots & \cos n_h t_0 & \sin n_h t_0\\
1 & \cos t_1 & \sin t_1 & \dots & \cos n_h t_1 & \sin n_h t_1\\
\vdots & \vdots & \vdots & & \vdots & \vdots\\
1 & \cos t_{2n_h} & \sin t_{2n_h} & \dots & \cos n_h t_{2n_h} & \sin n_h t_{2n_h}
\end{pmatrix}.$$

References

Hall, K.C., Thomas, J.P., Clark, W.S., 2002. Computation of unsteady nonlinear flows in cascades using a harmonic balance technique. AIAA Journal 40, 879–886.

Jones, R.T., 1940. The unsteady lift of a wing of finite aspect ratio. NACA Report 681

Lee, B.H.K., Gong, L., Wong, Y.S., 1997. Analysis and computation of nonlinear dynamic response of a two-degree-of-freedom system and its application in aeroelasticity. Journal of Fluids and Structures 11, 225–246.

Lee, B.H.K., Jiang, L.Y., Wong, Y.S., 1999a. Flutter of an airfoil with a cubic nonlinear restoring force. Journal of Fluids and Structures 13, 75–101.

Lee, B.H.K., Price, S.J., Wong, Y.S., 1999b. Nonlinear aeroelastic analysis of airfoils: bifurcation and chaos. Progress in Aerospace Science 35, 205–334.

Lee, B.H.K., Liu, L., Chung, K.W., 2003. Airfoil motion in subsonic flow with strong cubic nonlinear restoring forces. Journal of Sound and Vibration 281, 699–717.

Liu, L., Dowell, E.H., 2004. The secondary bifurcation of an aeroelastic airfoil motion: effect of high harmonics. Nonlinear Dynamics 37, 31–49.

Liu, L., Dowell, E.H., Thomas, J.P., Attar, P. and Hall, K.C., 2006. A comparison of classical and high dimensional harmonic balance approaches for a Duffing oscillator, Journal of Computational Physics 215, 298–320.

Price, S.J., Alighanbari, H., Lee, B.H.K., 1995. The aeroelastic response of a two-dimensional airfoil with bilinear and cubic structural nonlinearities. Journal of Fluids and Structures 9, 175–193.

Shen, S.F., 1959. An approximate analysis of nonlinear flutter problems. Journal of Aerospace Science 26, 25–32.

Thomas, J.P., Dowell, E.H., Hall, K.C., 2002a. Nonlinear inviscid aerodynamic effects on transonic divergence, flutter, and limit-cycle oscillations. AIAA Journal 40, 638–646.

Thomas, J.P., Dowell, E.H., Hall, K.C., 2002b. Modeling viscous transonic limit cycle oscillation behavior using a harmonic balance approach. AIAA Paper 2002–1414.

Woolston, D.S., Runyan, H.L., and Byrdsong, T.A., 1955. Some effects of system nonlinearities in the problem of aircraft flutter. NACA TN 3539.

Zhao, L.C., Yang, Z.C., 1990. Chaotic motions of an airfoil with nonlinear stiffness in incompressible flow. Journal of Sound and Vibration 138, 245–254.